ESLAB #53: The *Gaia* Universe
Edited by J.H.J. de Bruijne

Long-period variables in the *Gaia* era

Nami Mowlavi[1,2],Michele Trabucchi[3], Thomas Lebzelter[4]

[1] Department of Astronomy, University of Geneva, Ch. des Maillettes 51, CH-1290 Versoix, Switzerland
[2] Department of Astronomy, Beijing Normal University, Beijing, China
[3] Dipartimento di Fisica e Astronomia Galileo Galilei Università di Padova, Vicolo dell'Osservatorio 3, I-35122 Padova, Italy
[4]University of Vienna, Department of Astrophysics, Tuerkenschanzstrasse 17, A1180 Vienna, Austria

Abstract

The second *Gaia* data release (DR2, spring 2018) included a unique all-sky catalogue of large-amplitude long-period variables (LPVs), that include Miras and semi-regular variables. These stars are on the Asymptotic Giant Branch (AGB), and are characterized by high luminosity, changing surface composition, and intense mass loss that make them of paramount importance for stellar, galactic, and extra-galactic studies.
An initial investigation of these data for LPVs in the Large Magellanic Cloud (LMC) has revealed the possibility to disentangle O-rich and C-rich stars using a combination of optical *Gaia* and infrared 2MASS photometry. The so-called *Gaia*-2MASS diagram constructed to achieve this has further been shown to enable the identification of sub-groups of asymptotic giant branch stars among the O-rich and C-rich LPVs.
Here, we extend this initial study of the *Gaia*-2MASS diagram to the Small Magellanic Cloud (SMC) and the Galaxy, and show that the remarkable properties found in the LMC also apply to these other stellar systems. Interesting features, moreover, emerge as a result of the different metallicities between the three stellar environments, which we highlight in this exploratory presentation of *Gaia*'s potential to study stellar populations harboring LPVs.
Finally, we look ahead to the future and highlight the power of the exploitation of *Gaia* RP spectra for the identification of carbon stars using solely *Gaia* data in forthcoming data releases.
These proceedings include three animated images that can be used as outreach materials.

1 Introduction

The asymptotic giant branch (AGB) stage is the final evolutionary phase of low- and intermediate-mass stars. During this phase of high luminosity (their brightness can increase those of Cepheids), the surface composition is chemically altered by deep convective mixing, and the star loses mass at a high rate (up to 10^{-4} $M_\odot$/yr). Due to this, AGB stars play a key role in stellar and galactic evolution. A further characteristics of this phase is a long period variability (from tens to above a thousand of days), which makes the star identified as a long-period variable (LPV). This, combined with their intrinsic red colors, allows to easily identify them in large-scale surveys. This is specifically true for the *Gaia* all-sky survey, which provides, among other data, photometry in a main broad G optical band and in two color bands, $G_{\rm BP}$ (blue) and $G_{\rm RP}$ (red).

In Gaia Data Release 2 (DR2), Mowlavi *et al.* (2018) presented a catalogue of 151'761 LPV candidates with G band variability amplitudes larger than 0.2 mag (amplitudes measured between the 5 and 95% quantiles). Despite the use of selection criteria that aimed at prioritizing low contamination over high completeness – the completeness was estimated to be less than 50% over the entire sky–, this DR2 catalog already doubled the number of known such large-amplitude LPVs at the time of publication. It thereby provided a unique unprecedented catalog for the study of populations of LPVs.

Among the first applications of this catalog, our group investigated the potential of combining the optical *Gaia* $G_{\rm BP}$ and $G_{\rm RP}$ photometry with infrared photometry from 2MASS. Lebzelter *et al.* (2018) demonstrated on the DR2 LPV candidates of the Large Magellanic Cloud (LMC) that a combination of visual and infrared Wesenheit functions ($W_{\rm RP,BP-RP} - W_{\rm K_s,J-K_s}$, hereafter called the *Gaia*-2MASS Wesenheit index $\Delta W(Gaia, 2{\rm MASS})$), allows to nicely identify subgroups of AGB stars according to their mass and chemistry. In particular, C-rich stars can be distinguished from O-rich stars in the so-called *Gaia*-2MASS diagram, which plots the absolute magnitude (we used $K_{\rm s}$ as it is less sensitive to both interstellar extinction and intrinsic LPV variability than G) versus the *Gaia*-2MASS Wesenheit index. Low-mass, intermediate-mass and massive AGB stars are further distinguished in this diagram among the O-rich candidates, as well as supergiants. This provides new opportunities for stellar populations studies (e.g. age, chemical composition) from the study of the sub-populations of LPVs harbored therein. The reader is referred to Lebzelter *et al.* (2018) for a presentation of the properties and potential usage of this new *Gaia*-2MASS diagram of LPVs.

This ESLAB #53 conference aimed at showing the unique advances made possible by *Gaia* DR2 in various fields of astrophysics. In this spirit, we show in these proceedings the potential of *Gaia* to study populations of LPVs using the approach introduced in Lebzelter *et al.* (2018), but extended to the entire DR2 catalog (the study in Lebzelter *et al.* (2018) was based on the restricted list of candidates published in the DR2 catalog of LPVs) and to various stellar environments (the study in Lebzelter *et al.* (2018) was limited to the LMC). To achieve this, we first need to be able to identify LPVs in

the entire DR2 archive. This is addressed in Sect. 2, and applied to the LMC in Sect. 3. Populations of LPVs in the Small Magellanic Cloud (SMC) and in the Galaxy are then explored using this technique in Sects. 4 and 5, respectively.

Given the paramount importance of the question of C-rich star identification for the chemical return of AGB stars and for the chemical evolution of the Galaxy (and of galaxies in general), we devote Sect. 6 to a brief presentation of the unique potential of *Gaia* in this respect. We already showed in Lebzelter *et al.* (2018) the possibility of this identification using the *Gaia*-2MASS diagram, as recalled above. Its application to the SMC and the Galaxy, in addition to the LMC, is discussed in Sect. 6.1. Yet, the potential of *Gaia* in its future data releases is expected to be even greater, with the provision of information extracted from the epoch RP spectra of the *Gaia* red spectro-photometer. This was shown in the *Gaia* Image of the Week (IoW) of 15/11/2018 published on the *Gaia* web pages of the European Space Agency (ESA)[1], and is recalled in Sect. 6.2. Section 7 finally ends these proceedings with some conclusions.

2 The sample of LPV candidates

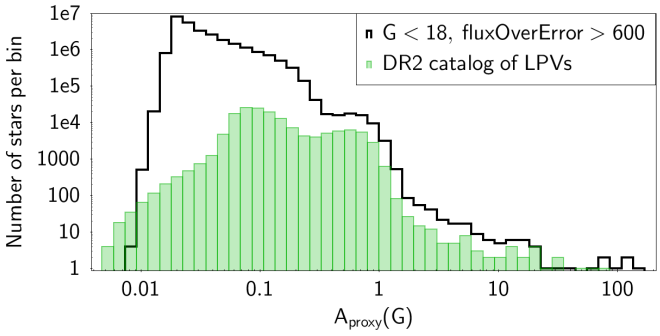

Figure 1: Black histogram: Distribution of the variability proxy in the set of all *Gaia* sources in the *Gaia* archive brighter than $G = 18$ mag and having flux(G)/fluxError(G)>600. Green histogram: Same as the black histogram, but for all sources in the *Gaia* DR2 catalog of LPV candidates.

Similarly to the sample selection done in the *Gaia* DR2 catalog of LPVs, we aim here at identifying all Gaia red giants with large variability amplitudes. The variability proxy used to achieve this is described in Sect. 2.1, and the procedure to select the data set of LPV candidates from the *Gaia* archive is described in Sect. 2.2.

2.1 Variability proxy

The G-band variability amplitude is provided in DR2 for all LPV candidates through either the standard deviation or the 5-95% quantile range $QR_5(G)$ of their G magnitude time series. These quantities are not available for the sources that have no variability-specific information in DR2. They cannot be computed neither, since the light curves are not published.

We can, however, make use of the published G flux uncertainties, which contains information both on the uncertainties of the individual measurements and on the intrinsic

[1]https://www.cosmos.esa.int/web/gaia/iow_20181115

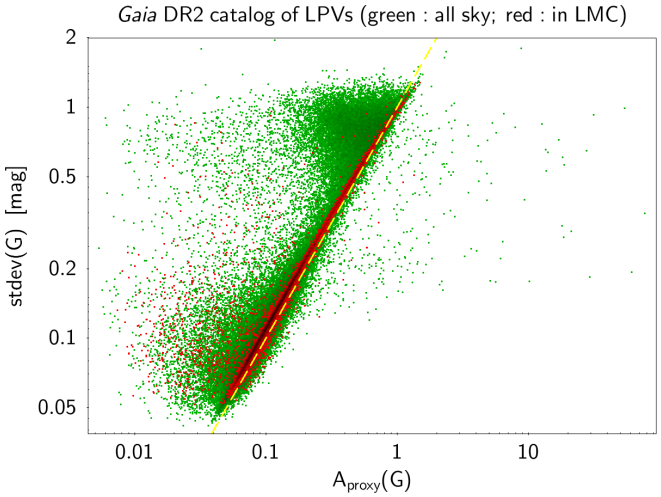

Figure 2: Variability proxy (X-axis) versus standard deviation of the G magnitude time series (Y-axis) for all LPV candidates published in *Gaia* DR2. The yellow dashed line is a diagonal line to guide the eye.

scatter of the flux time series (see Sect. 5.3.5 of the Gaia DR2 documentation in Busso *et al.*, 2018). Since the intrinsic scatter of large-amplitude LPVs is much larger (≥ 0.2 mag) than the typical few milli-magnitude level photometric uncertainties at the magnitudes considered for LPVs ($G \leq 16$ mag), the flux uncertainty can be used as a good proxy $A_{\rm proxy}(G)$ of the intrinsic standard deviation of their light curves using the following formula:

$$A_{\rm proxy}(G) = \sqrt{N_{\rm obs}}\, \varepsilon(F(G))/F(G)\ , \qquad (1)$$

where $N_{\rm obs}$ is the number of (per-CCD) observations, $F(G)$ the G-band flux, and $\varepsilon(F(G))$ its quoted error. All quantities entering Eq. 1 are available in DR2. This approach was already used by Deason *et al.* (2017) to identify Mira variables in *Gaia* DR1.

The relation between $A_{\rm proxy}(G)$ and the standard deviation of the G magnitude time series is shown in Fig. 1 to be an almnost one-to-one relation, except for a subset of the sources which have a value of their (flux-based) variability proxy smaller than their (magnitude-based) standard deviation (only very few sources have their variability proxy larger than their magnitude-based standard deviation).

The relation between variability proxy and 5-95% quantile range $QR_5(G)$ used in DR2 to characterize the variability amplitudes of LPVs is shown in Fig. 3. The majority of sources are close to the linear relation $QR_5(G) = 3.3 * A_{\rm proxy}(G)$. Sources that deviate from the linear relation have a far-from-optimal sampling of measurements. For the majority of these sources, the standard deviation (and hence the variability proxy) underestimates the variability range. For example, for sources in the LMC shown in red in Fig. 3, the standard deviation of the sources close to the South Ecliptic Pole will have too small standard deviations due to the large number of measurements during the one-month EPSL observation compared to the standard deviations they would have if they had a regular sampling over their pulsation phases.

Miras, which pulsate in the fundamental mode, were

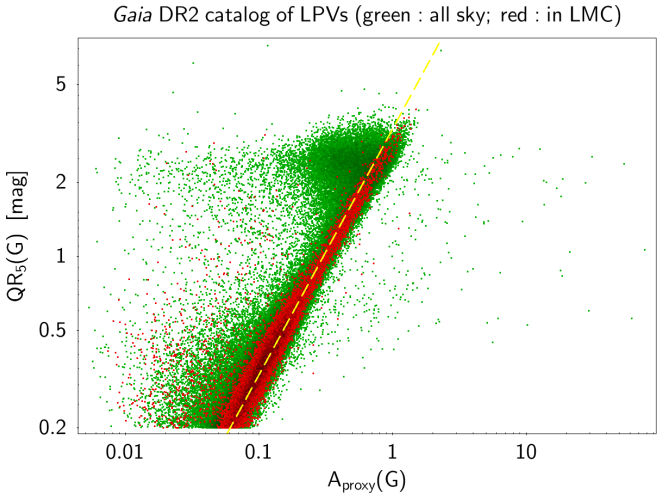

Figure 3: Same as Fig. 2, but with variability proxy plotted versus 5-95% quantile range of the G magnitude time series. The yellow dashed line is a $y = 3.3\,x$ relation.

shown in Mowlavi *et al.* (2018) to have $QR_5(G) \gtrsim 1$ mag. This translates to $A_{\rm proxy}(G) \gtrsim 0.3$. LPVs with $A_{\rm proxy}(G) \lesssim 0.3$, on the other hand, will mainly consist of semi-regular variables (SRVs), pulsating in overtone modes.

The variables with the largest amplitudes ($A_{\rm proxy}(G) > 0.3$) mainly consist of Mira candidates, which pulsate in the fundamental mode, while the smaller amplitude LPVs are mainly semi-regular variables (SRVs), pulsating in overtone mode(s).

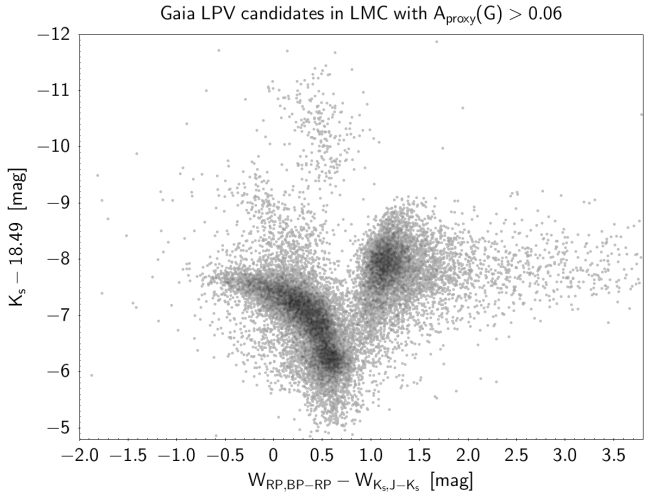

Figure 4: *Gaia*-2MASS diagram of the LPV candidates in the LMC selected from the full DR2 archive with the condition $A_{proxy} > 0.06$ on the variability proxy and $J < 14.5$ mag, $K_{\rm s} < 14.5$ mag on 2MASS photometry of the cross matches.

2.2 The data

Since the variability proxy is not an indexed column in the Gaia archive, and thus cannot be used to extract samples of sources from the archive, we downloaded all sources with flux(G)/fluxError(G)>600. It contains 27'170'927 sources. A comparison of the variability proxy distribution in this sample with the distribution in the DR2 catalog of LPVs (Fig. 1) shows that this criterion allows to retrieve the great majority of sources present in the latter catalog, which contained sources with a minimum variability amplitude of $QR_5(G) = 0.2$ mag. 148'714 of the 151'761 sources in the DR2 catalog of LPVs (i.e. 98% of them) are retrieved in this way.

In these proceedings, we select as LPV candidates all Gaia DR2 red sources ($G_{\rm BP} - G_{\rm RP} > 1.5$ mag) that have a variability proxy $A_{\rm proxy}(G) > 0.06$ mag. This limit was selected to comply with the amplitude limit ($QR_5(G) > 0.2$ mag) set for DR2. We further restrict the sample to sources that have 2MASS crossmatches with $J < 14.5$ mag and $K_{\rm s} < 14.5$ mag. These conditions on the 2MASS photometry are intended to provide near-infrared data with good quality to construct *Gaia*-2MASS diagrams.

The final sample of LPV candidates selected in the above way from the entire DR2 archive contains 2'075'586 *Gaia* DR2 sources distributed all over the sky.

3 LPVs in the Large Magellanic Cloud

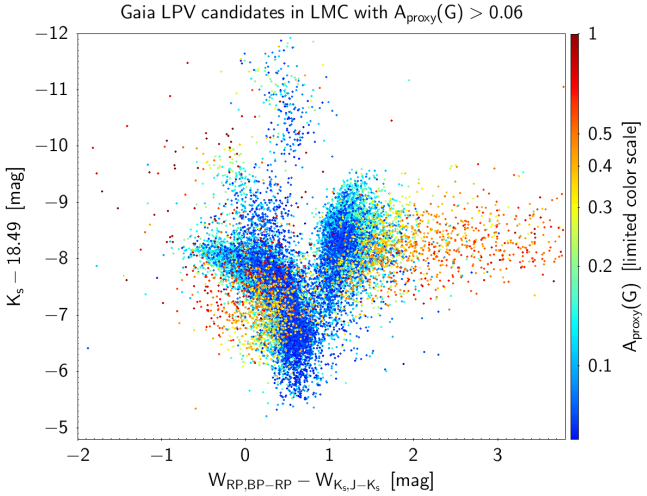

Figure 5: Sources with $A_{\rm proxy}(G) < 0.06$ or $A_{\rm proxy}(G) > 1$ are plotted with the color at the respective end of the color-scale. The subset of sources with $A_{\rm proxy}(G) > 0.3$ has been plotted on top of the subset with $A_{\rm proxy}(G) < 0.3$ to ensure that the former ones are all shown on top of the latter ones on the figure.

Members of the LMC are selected on the basis of their location in the sky, their proper motions, and their parallax. The selection criteria are the same as the ones used in Lebzelter *et al.* (2018), recalled in Table 1. With the additional condi-

criteria	LMC sample	SMC sample
RA	50° to 105°	0° to 35°
DEC	−77° to −61°	−80° to −65°
PM(RA)	1.2 to 2.5 mas/yr	−0.3 to 1.6 mas/yr
PM(DEC)	−0.8 to 1.5 mas/yr	−1.9 to −0.7 mas/yr
ϖ	< 0.5 arcsec	< 0.5 arcsec

Table 1: Selection criteria for stars in the LMC and SMC.

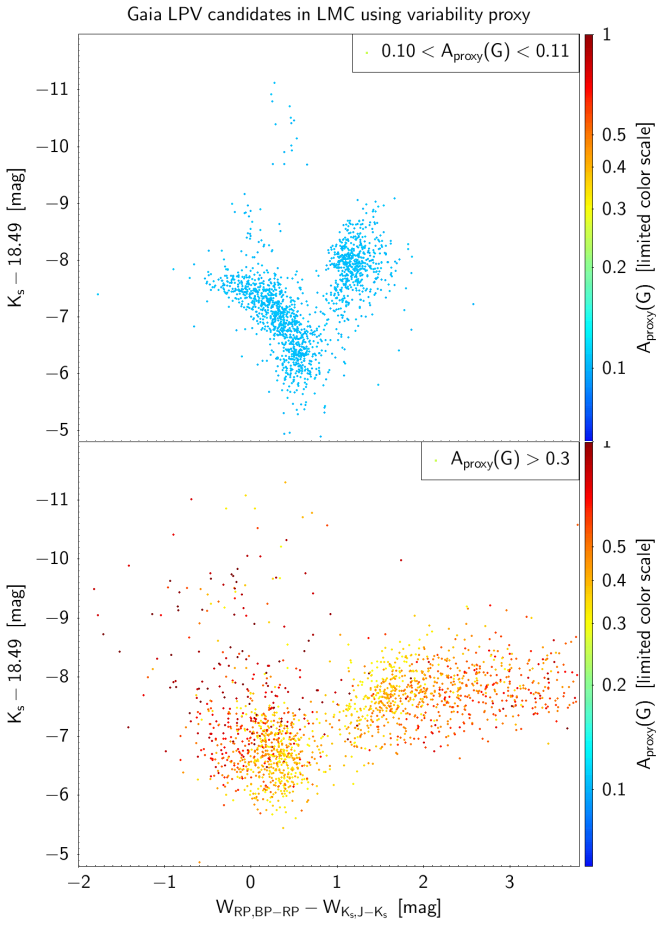

Figure 6: Same as Fig. 5, but with restricted variability proxy ranges. The top panel is restricted to $0.10 < A_{\rm proxy}(G) < 0.11$ (containing mainly SRVs), while the bottom panel covers $A_{\rm proxy}(G) > 0.3$ (containing only Miras).

tions mentioned in Sect. 2.2 on *Gaia* color, variability proxy and 2MASS photometry, the sample of LPVs in the LMC amounts to 20'486 sources. This is almost twice the number of sources (10'989 sources) of the LMC published in the *Gaia* DR2 catalog of LPV candidates.

The distribution in the *Gaia*-2MASS diagram of these LMC LPV candidates is shown in Fig. 4. The various branches related to different stellar mass regimes that were detected by Lebzelter *et al.* (2018) are clearly visible for this larger sample as well.

Fig. 5 shows the same diagram, but with a color index according to $A_{\rm proxy}(G)$ values of the stars. Mira candidates are plotted on top of the other stars to make them all visible. Their distribution in the diagram seems to follow a slightly different pattern than the smaller amplitude SRVs, with Miras spreading more over the diagram than SRVs. This is more clearly shown in Fig. 6, which separates the two groups of stars, Mira candidates and SRV candidates, in the top and bottom panels, respectively. The discussion on this feature must distinguish the case of C-rich stars (right half of the diagram at $\Delta W(Gaia, 2{\rm MASS}) \gtrsim 0.8$ mag) from the case of O-rich stars (left half of the diagram).

The C-rich Miras in Fig. 6 (bottom panel) extend towards

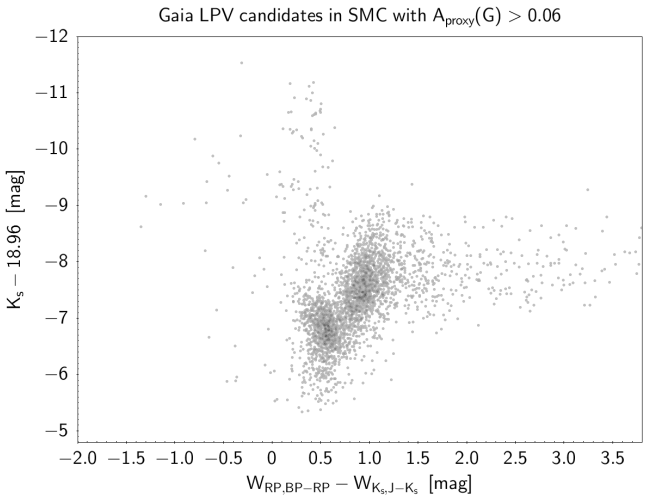

Figure 7: Same as Fig. 4, but for the SMC.

very large $\Delta W(Gaia, 2{\rm MASS})$ values compared to the SRVs (top panel). In Lebzelter *et al.* (2018), we named these stars 'extreme C-stars', and we suggested that these are high-mass-loss objects. The fact that only large amplitude variables are found here confirms the widely accepted connection between large amplitude variability and mass loss (e.g. Höfner & Olofsson, 2018).

Concerning the M-type Miras, many of them are found below the lowest luminosity branch in Fig. 5 (branch (a) in Lebzelter *et al.*, 2018). A detailed analysis of this group is beyond the scope of this proceedings paper. However, we note that circumstellar reddening resulting from heavy mass loss (see, e.g., McDonald *et al.*, 2018) and the appearance of significant amounts of water absorption in the near-infrared spectra (see Fig. 2 in Aringer *et al.*, 2002) are expected to reduce the $K_{\rm s}$ band brightness of these stars. Furthermore, the $K_{\rm s}$-band magnitudes used here are single-epoch observations, so that we expect to see a larger scatter in $K_{\rm s}$ for large-amplitude stars. These effects affect less SRVs because they have, on average, less circumstellar reddening, and because their amplitude of variability is smaller than for Miras. The effects also lead to a spread of the $\Delta W(Gaia, 2{\rm MASS})$ values of Miras, but to a lesser degree because the Wesenheit index partly corrects for the reddening effect. In summary, the $K_{\rm s}$ magnitude of O-rich Miras is expected to be, on the mean, larger (fainter) than that of O-rich SRVs, and to display a larger spread due to their larger intrinsic variability amplitude combined to the single-epoch nature of the 2MASS survey.

4 LPVs in the Small Magellanic Cloud

The selection criteria for members of the SMC are given in Table 1. With the additional conditions on *Gaia* color, variability proxy, and 2MASS photometry mentioned in Sect. 2.2 to select large-amplitude LPV candidates, we reach a sample of 3'208 sources.

The *Gaia*-2MASS diagrams for the SMC are shown in Figs. 7 and 8. There are two main differences compared to the equivalent diagrams for the LMC (Figs. 4 and 5, respectively). First is the larger proportion of C-rich over O-rich stars in the SMC than in the LMC. This is a well known fact, due to the

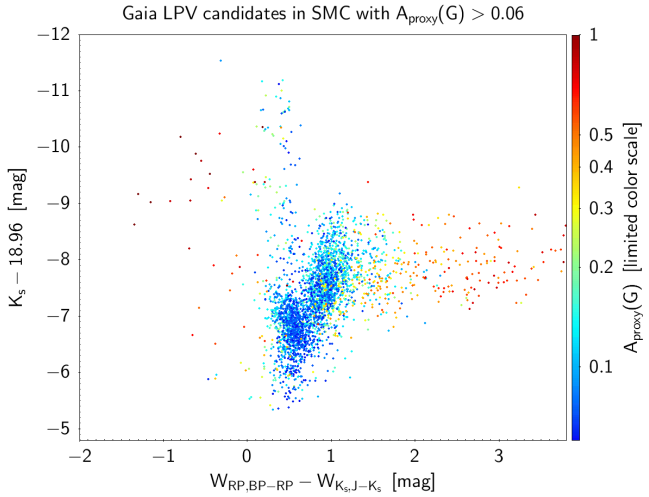

Figure 8: Same as Fig. 5, but for the SMC.

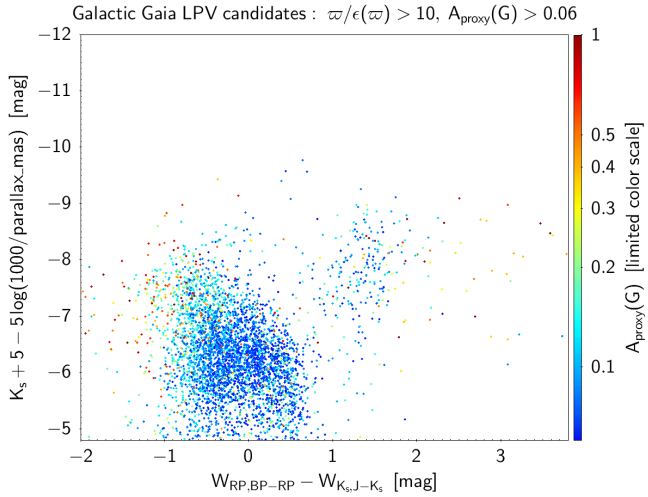

Figure 9: Same as Fig. 5, but for Galactic LPVs with a relative DR2 uncertainty on the parallaxes better than 10%.

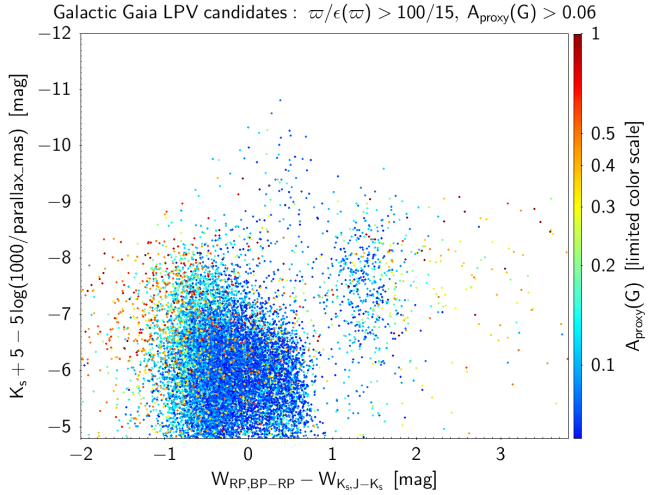

Figure 10: Same as Fig. 5, but for Galactic LPVs with a relative DR2 uncertainty on the parallaxes better than 15%.

lower metallicity of the SMC in which AGB stars more easily experience third dredge-up and at an earlier stage on their AGB phase, combined with the lower oxygen abundance in the atmosphere of an SMC AGB star such that a smaller number of dredge-up events is needed to reach C/O>1. As a result, the star spends an increased fraction of its lifetime as a C-star (see, e.g., Fig. 22 in Marigo & Girardi, 2007). Similar conclusions are drawn in the literature from, for example, the observation of stellar clusters in the SMC (Frogel *et al.*, 1990), or the analysis of the period-luminosity diagram of LPVs in the SMC (Soszyński *et al.*, 2011).

The second striking feature in Fig. 7 of the SMC compared to Fig. 4 of the LMC is the truncation of the O-rich low-mass branch towards low $\Delta W(Gaia, 2\mathrm{MASS})$ values: there is practically no LPV with $\Delta W(Gaia, 2\mathrm{MASS}) < 0.2$ mag. This may be a direct consequence of the increase of third dredge-up efficient with decreasing metallicity, the O-rich star turning into a C-rich star before it moves far to the left of the *Gaia*-2MASS diagram.

Let us, however, remark that the specific star formation history of the SMC, a subtle interplay between metallicity and evolution, the larger surface temperatures usually characterizing lower metallicity stars, and/or the smaller Ti abundance due to the smaller metallicity, all could play a role in shaping the distribution of O-rich LPVs in the *Gaia*-2MASS diagram. We further note from Fig. 8 that almost all O-rich stars beyond the truncation limit of branch (a) on the left of the diagram, with $\Delta W(Gaia, 2\mathrm{MASS}) < 0.2$ mag, are Miras.

5 LPVs in the Galaxy

The study of LPVs in the Galaxy is much more challenging than in the Magellanic Clouds. First, because they cannot be assumed to be at a given known distance as is the case for the LMC and the SMC. Here *Gaia* will be of key help by providing parallax measurements. Second, because Galactic sources are affected by differential interstellar reddening that varies greatly on the sky position and distance into the Galaxy.

We consider two samples of Galactic LPVs, selected according to the relative uncertainty on their parallaxes. The first sample is restricted to all LPV candidates (selected with the criteria on color, variability amplitude and 2MASS photometry precision as described in Sect. 2.2) with relative *Gaia* DR2 parallax uncertainties better than 10%, while the second sample contains a larger set with parallax uncertainties up to 15%. In both samples, we have to exclude potential Young Stellar Objects that can be contaminants to LPVs (see Mowlavi *et al.*, 2018). We do this by imposing an upper limit on the absolute(G) magnitude of LPVs, that depends on the G_{BP}-G_{RP} color as defined by the dashed line in the Fig. 28 of Mowlavi *et al.* (2018), i.e. absolute$(G) < -2.6 + 1.72 * (G_{\mathrm{BP}} - G_{\mathrm{RP}})$.

The *Gaia*-2MASS diagrams of these two samples of Galactic LPV candidates are shown in Figs. 9 and 10, respectively. We note the following points:

- There are much less C-rich relative to O-rich stars in the Galaxy than in the Clouds (compare Fig. 9 with Fig. 7. This is in agreement with the predicted decrease of ef-

ficiency of third dredge-up with increasing metallicity combined with the larger O abundance in the envelope of the AGB star, as already noticed in Sect. 4 when comparing the representative diagrams of the SMC and LMC.

- The distribution of O-rich LPVs in branch (a) of the diagram (containing low-mass AGB stars as well as stars at the tip of the red giant branch) covers, at any given absolute K_s magnitude, a much wider range of $\Delta W(Gaia, 2\mathrm{MASS})$ in the Galaxy than in the Clouds. In Sect. 4, we noticed a truncated extension of branch (a) in the SMC compared to the LMC. If this observed difference can be extrapolated to the larger metallicity of the Galaxy, we would expect $\Delta W(Gaia, 2\mathrm{MASS})$ to be smaller (i.e. larger negative values) in the Galaxy than in the LMC, as observed here. Interstellar (and possibly circumstellar) reddening would then explain the distribution of branch (a) in Figs. 9 and 10 towards the faint (lower) side of the diagram. The wide distribution of branch (a) for the Galaxy, in both the X and Y axes, would thus result from the combined effect of O-rich AGB stars turning much later into C-rich stars, if at all, (plus other potential sources of the effect as discussed in Sect. 4) and extinction. But see also the note at the end of this section on parallax determinations.

- Despite the previous point, the group of C-rich stars stand still distinctly from the group of O-rich stars in Figs. 9 and 10. This remarkable property of the *Gaia*-2MASS diagram results from the fact that reddening leads to a slight displacement of the representing point in the diagram *away* from the vertical line separating the two groups of stars: a reddened C-rich star will be displaced to larger $\Delta W(Gaia, 2\mathrm{MASS})$, while reddened O-rich stars will be displaced to smaller (negative) values of this index.

- Only very few massive AGB and red supergiants are present in the Galactic sample.

Let us finally issue a warning on the parallaxes. Attention must be taken that systematics and biases may exist in the DR2 parallaxes determinations of red giants. A bias towards the exclusion of the reddest giants in a parallax precision-limited sample was already stressed in Mowlavi *et al.* (2018) (see in particular their Fig. 24), due to their fainter magnitudes (maximum of spectrum emission displaced to longer wavelengths in the infrared). In addition, there were limitations in DR2 parallaxes (Lindegren *et al.*, 2018).

6 C-star identification

6.1 In the *Gaia*-2MASS diagram

With the DR2 *Gaia* data, Lebzelter *et al.* (2018) showed how the combination of optical with infrared data allows to distinguish between O-rich and C-rich stars in the *Gaia*-2MASS diagram, where these two types of LPVs occupy distinct regions. It was shown that this optical+infrared diagram is more powerful than the infrared color-magnitude diagram usually used in the literature for this purpose. The improvement is illustrated in Fig. 12, for which an animated image is available (see caption of the figure).

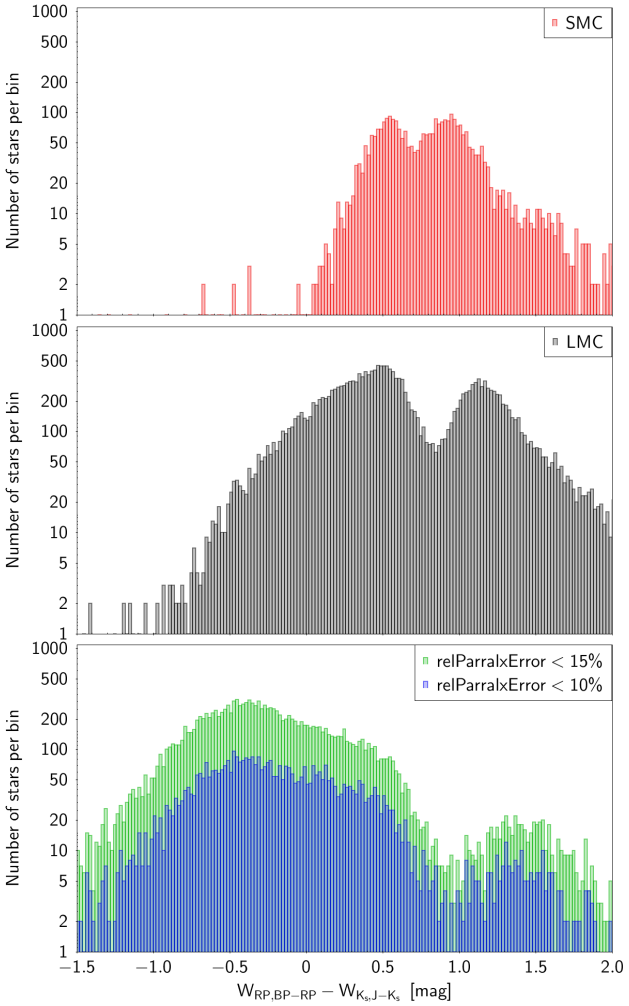

Figure 11: Histogram of $\Delta W(Gaia, 2\mathrm{MASS}) = W_{\mathrm{RP,BP-RP}} - W_{\mathrm{K_s,J-K_s}}$ for all *Gaia* DR2 LPV candidates with $A_{\mathrm{proxy}}(G) > 0.06$ in the SMC (top panel), LMC (middle panel) and Galaxy (bottom panel, for stars with relative parallax uncertainty better than 10% in blue and than 15% in green).

With the samples of *Gaia* sources prepared in the previous sections to study the populations of LPVs in the SMC, LMC and in the Galaxy, we can investigate whether the delineation between C-rich and O-rich LPVs in the *Gaia*-2MASS diagram depends on metallicity. For this purpose, the histograms of $\Delta W(Gaia, 2\mathrm{MASS})$ for the SMC, LMC and Galactic vicinity are shown in Fig. 11, respectively from top to bottom. The value of $\Delta W(Gaia, 2\mathrm{MASS})$ at the minimum of the histograms approximately delineates the border between O-rich (values smaller than this limit) and C-rich (values larger than this limit). The exact value actually depends on the absolute K_s magnitude, the border not being a straight vertical line in the *Gaia*-2MASS diagram. The differences between the histograms of the different stellar populations nevertheless suggest a slight metallicity dependence of the borders separating the different subgroups of AGB stars, this border shifting to slightly larger values with an increase of the metallicity of the considered stellar population. Further studies, outside the

scope of these proceedings, should be performed on the full 2D distribution of sources in the *Gaia*-2MASS diagrams, and distinguishing the various stellar populations in the Galaxy (halo, thin/thick disk, bulge), in order to reach a full understanding of the metallicity dependence of the boarders between the different regions in this diagram.

6.2 Using solely *Gaia* data

The next *Gaia* data releases offer new perspectives for the identification of C stars. The red spectro-photometer on board of *Gaia* indeed provides low-resolution spectra that are adequate for a discrimination between O-rich and C-rich stars, from the signature of molecular bands specific to either O-rich (mainly TiO and VO) or C-rich (mainly C_2, CH, and CN) cool stellar atmospheres. This was shown in the *Gaia* IoW released on Nov. 15, 2018, on ESA's *Gaia* web pages, which shows the epoch RP spectra of two Miras, the O-rich Mira T Aqr (pulsation period of $P = 203$ d) and the C-rich Mira RU Vir ($P = 425$ d). The displayed epoch spectra reveal significant variations of the shapes of the spectra as a function of pulsation phase, due to stellar surface temperature changes of these large amplitude Miras. A method was also described in the IoW to make use of the features present in the RP spectra to distinguish C-rich from O-rich stars. The reader is referred to the explanations provided therein for more information.

Here, we link the variations of the RP spectra of T Aqr and RU Vir with their photometric variability. The spectra are taken from the IoW, and the photometric light curves are downloaded from the *Gaia* DR2 archive. The results are shown in Figs. 13 and 14, respectively.

7 Conclusions

Gaia DR2 has shown the potential of *Gaia* to revolutionize the study of stellar populations harboring LPVs, and the next data releases are expected to be even more promising when the data from all *Gaia* instruments will be fully exploited.

Acknowledgments

We thank Dr. Maria Süveges for her help in the preparation of the *Gaia* RP spectra data published in the *Gaia* Image of the Week of 15/11/2018.

References

Aringer, B., Kerschbaum, F., & Jörgensen, U. G. 2002, A&A, 395, 915.

Busso, G., Cacciari, C., Carrasco, J. M., De Angeli, F., Evans, D. W., *et al.* 2018, *Gaia DR2 documentation Chapter 5: Photometry.* Tech. rep.

Deason, A. J., Belokurov, V., Erkal, D., Koposov, S. E., & Mackey, D. 2017, MNRAS, 467, 2636.

Frogel, J. A., Mould, J., & Blanco, V. M. 1990, ApJ, 352, 96.

Höfner, S. & Olofsson, H. 2018, A&ARv, 26, 1.

Lebzelter, T., Mowlavi, N., Marigo, P., Pastorelli, G., Trabucchi, M., *et al.* 2018, A&A, 616, L13.

Lindegren, L., Hernández, J., Bombrun, A., Klioner, S., Bastian, U., *et al.* 2018, A&A, 616, A2.

Marigo, P. & Girardi, L. 2007, A&A, 469, 239.

McDonald, I., De Beck, E., Zijlstra, A. A., & Lagadec, E. 2018, MNRAS, 481, 4984.

Mowlavi, N., Lecoeur-Taïbi, I., Lebzelter, T., Rimoldini, L., Lorenz, D., *et al.* 2018, A&A, 618, A58.

Soszyński, I., Udalski, A., Szymański, M. K., Kubiak, M., Pietrzyński, G., *et al.* 2011, AcA, 61, 217.

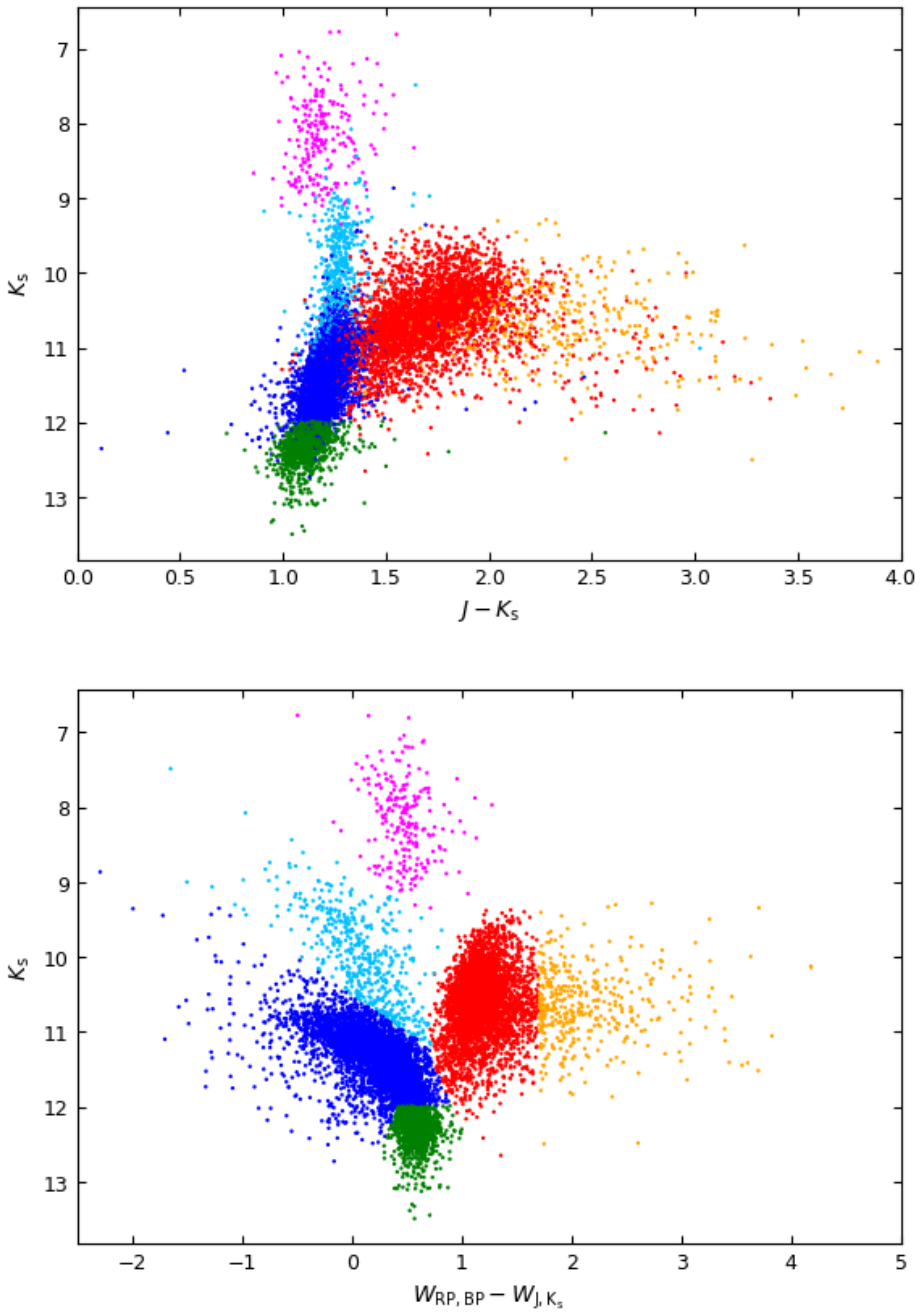

Figure 12: Distribution of the LMC LPV candidates from the *Gaia* DR2 catalog of LPVs in the 2MASS color-magnitude diagram (top panel, units of both axes in magnitude) compared to their distribution in the *Gaia*-2MASS diagram (bottom panel, units of both axes in magnitude). The colors indicate the different subgroups of AGB stars identified in Lebzelter *et al.* (2018).
An animated image illustrating the shift from the left to the right diagrams is available at `https://obswww.unige.ch/~mowlavi/OnlineMaterial/Images/figAnimated_Gaia2MASS_diagram.gif`. Any future change of the location on the web of this animated image will be indicated in an updated version of these proceedings on arXiv.org e-Print archive (`https://arxiv.org/archive/astro-ph`).

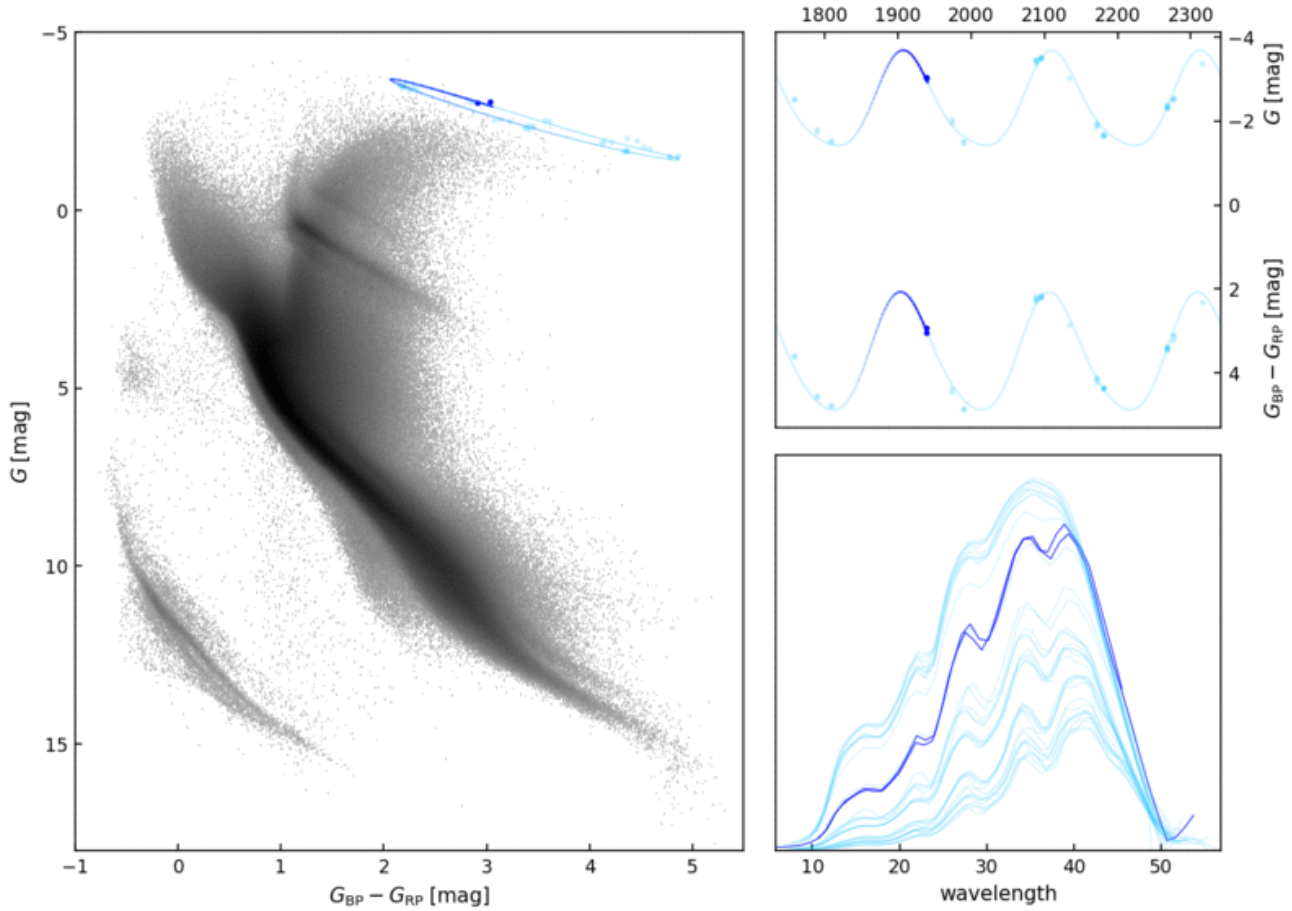

Figure 13: Photometric and spectroscopic variability of the O-rich Mira T Aqr ($P = 203$ d) during the 22 months of data covered by *Gaia* DR2. **Left panel:** Photometric variability of the star (in blue) in the *Gaia* color – Absolute magnitude diagram. The background stars are the set of *Gaia* DR2 sources brighter than $G = 18$ with $\varpi/\varepsilon(\varpi) > 30$ and good BP+RP excess factors. **Right top panel:** Time series of the G magnitude and $G_{\rm BP}$-$G_{\rm RP}$ color of the star. The times on the X-axis are given in days. **Right bottom panel:** Epoch RP spectra of the star. The X-axis is a pseudo-wavelength covering the approximate range from 640 to 1100 nm). The Y-axis represents fluxes with a range from 0 to $\sim 1.5 \times 10^6$ e$^-$/s/sample. The dark blue point/spectrum in each panel identifies the same given time.
An animated image illustrating the variability of the star with time is available at `https://obswww.unige.ch/~mowlavi/OnlineMaterial/Images/figAnimated_TAqr_Mtype.gif`. Any future change of the location on the web of this animated image will be indicated in an updated version of these proceedings on arXiv.org e-Print archive (`https://arxiv.org/archive/astro-ph`).

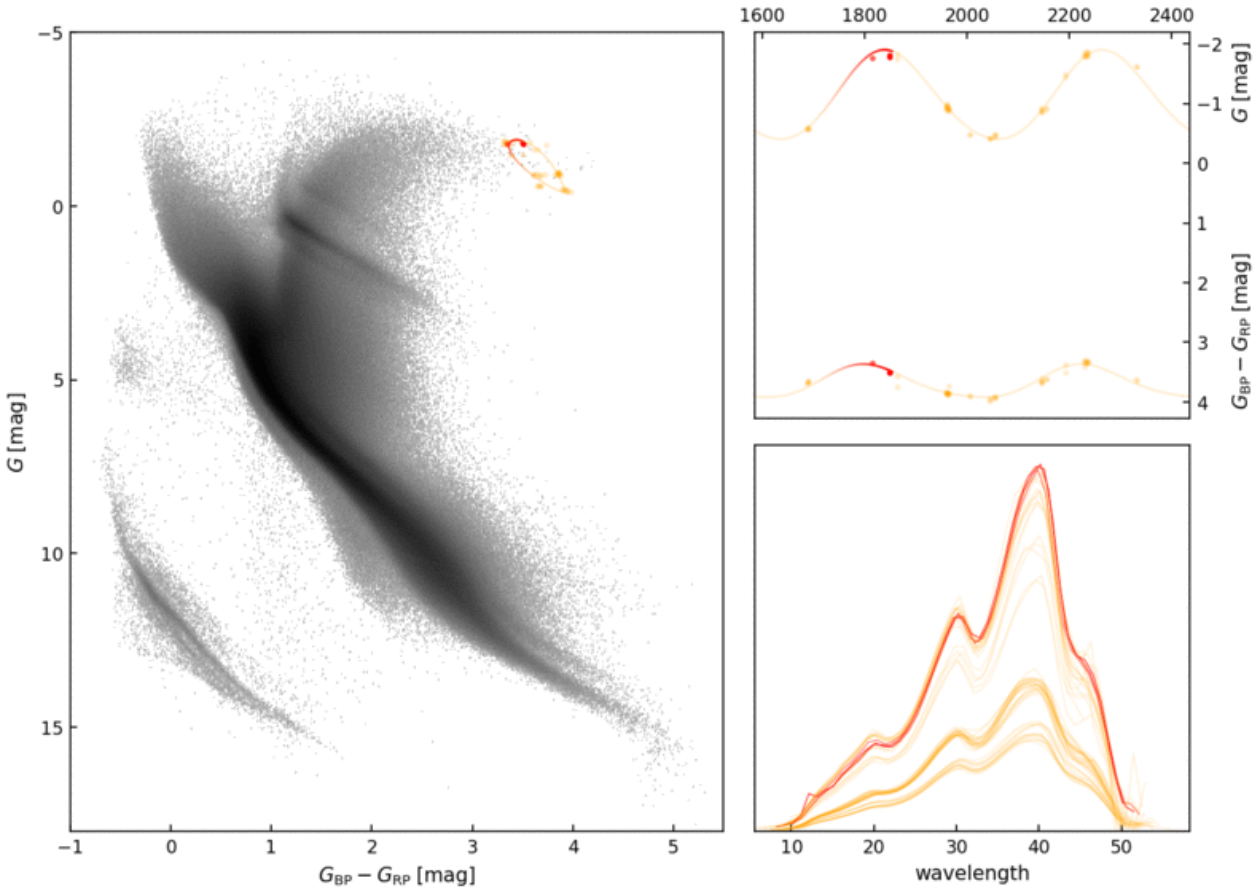

Figure 14: Same as Fig. 13, but for the C-rich Mira RU Vir ($P = 425$ d). The Y-axis represents fluxes with a range from 0 to $\sim 0.8 \times 10^6$ e^-/s/sample. The blue color of Fig. 13 has been replaced by red color in all panels.
An animated image illustrating the variability of the star with time is available at `https://obswww.unige.ch/~mowlavi/OnlineMaterial/Images/figAnimated_RUVir_Ctype.gif`. Any future change of the location on the web of this animated image will be indicated in an updated version of these proceedings on arXiv.org e-Print archive (`https://arxiv.org/archive/astro-ph`).